

# Low-temperature preparation of ZnO thin film by atmospheric mist chemistry vapor deposition for flexible organic solar cells

Jiang Cheng<sup>1,2</sup> · Qi Wang<sup>2</sup> · Chengxi Zhang<sup>2</sup> · Xin Yang<sup>1,2</sup> · Rong Hu<sup>2</sup> ·  
Jiang Huang<sup>1</sup> · Junsheng Yu<sup>1,2</sup> · Lu Li<sup>2</sup>

Received: 22 November 2015 / Accepted: 7 March 2016 / Published online: 17 March 2016  
© Springer Science+Business Media New York 2016

**Abstract** A low-temperature method for the large-scale growth of ZnO thin films on flexible substrates was realized using a mist chemistry vapor deposition setup. We prepared and analyzed ZnO thin films grown on flexible PET/ITO in the temperatures range of 125–250 °C. The growth of ZnO crystallites was qualitatively investigated with respect to nucleation and substrate temperature. We observed a mixed phase in the ZnO thin films prepared at 125 and 150 °C. We conclude that the optimal substrate temperature for optimal ZnO thin films growth is between 150–200 °C. Our results show that the photovoltaic performance of an organic solar cell (OSC) is strongly dependent on both composition and morphology. To demonstrate its application on flexible organic optoelectronic devices, a large OSC with as-grown ZnO thin film as cathode buffer layer was successfully prepared.

## 1 Introduction

Flexible organic devices including flexible organic light-emitting diodes (OLEDs) and organic solar cells (OSCs) have received a great deal of attention due to their low cost

and suitability for flexible display applications and wearable electronic devices. Multifunctional ZnO thin films are widely used as cathode buffer layers (CBLs) in OLEDs [1] OFETs [2] and OSCs [3] devices. They can improve both the electron collection and transport efficiency by selecting negative carriers and blocking positive carriers [4, 5].

ZnO thin films can be grown using several methods including magnetron sputtering [6], chemical vapor deposition (CVD) [7], atom layer deposition (ALD) [8], and the sol–gel approach [9]. Compared to vacuum deposition, solution processing techniques including spin-coating and MICVD are particularly attractive as they represent a cheap way of preparing large-scale ZnO thin films under ambient conditions. For this method, a low growth-temperature is crucial to ensure compatibility with flexible device fabrication and roll-to-roll processing. However, it is well known that low-temperature growth is difficult to achieve in non-vacuum processes since the thermal energy is a prerequisite for decomposing zinc salt solutions. For example, traditional MICVD using zinc acetate or zinc nitrate solution requires a substrate temperature higher than 320 °C to enable crystallization [10, 11]. Much research effort has been devoted to decrease the growth temperature. Recently, ZnO thin films grown from zinc acetylacetonate ethanol solution at a only 200 °C have been reported [12, 13]. Unfortunately, this temperature is still not low enough for the growth to produce high quality ZnO thin films on most flexible transparent substrates. Nevertheless, ZnO thin films could be prepared on flexible substrates at 100 °C using a diethylzinc (DEZ) solution [14, 15]. Unfortunately, the toxicity and instability of DEZ leads to serious safety and health problems for operators and the environment, which limits its practical use.

In this paper, we have used a low-decomposition-temperature zinc–ammonia  $[\text{Zn}(\text{NH}_3)_4](\text{OH})_2$  solution as a

✉ Junsheng Yu  
jsyu@uestc.edu.cn

✉ Lu Li  
lli@cqwu.edu.cn

<sup>1</sup> State Key Laboratory of Electronic Thin Films and Integrated Devices, School of Optoelectronic Information, University of Electronic Science and Technology of China, Chengdu 610054, People's Republic of China

<sup>2</sup> Co-Innovation Center for Micro/Nano Optoelectronic Materials and Devices, Research Institute for New Materials and Technology, Chongqing University of Arts and Sciences, Chongqing 402160, People's Republic of China

precursor for the ZnO thin films. With a self-designed simple and a cost-effective apparatus, large scale ZnO thin films were grown on flexible substrates at a very low temperature and ambient conditions. The effect of substrate temperature on composition, crystal structure, morphology, and optical properties as well as the performance of OSCs are also discussed.

## 2 Experiment details

A zinc–ammonia precursor was prepared using the following steps. 5 g zinc acetate was dissolved in 150 ml deionized H<sub>2</sub>O. The solution was then completely precipitated by dropping in 3.5 ml NH<sub>3</sub>·H<sub>2</sub>O. The mixture was vacuum-filtrated and then washed by more than 1 l of deionized water in order to remove CH<sub>3</sub>COO<sup>−</sup>. Finally, the precipitate was dissolved in 50 ml of ammonia–water, and then diluted with 100 ml deionized water and a 50 ml methanol mixture.

The MICVD setup comprises an ultrasonic transducer, an automatic X–Y table, a heating block, and pipe fittings. The purpose of the ultrasonic transducer is to generate an ultrasonic wave, which continuously converts solution into mist. Glass/ITO (8 Ω/square) and flexible PET/ITO (40 Ω/square) substrates were used. During the deposition process, a Φ 20 mm nozzle was mounted 10 mm above the heating block. Compressed air was used as the carrier gas and was held at a flow rate of 10 L min<sup>−1</sup>. The solution atomization rate was approximately 3 ml min<sup>−1</sup>. In this study, we investigate the growth of ZnO thin films on PET/ITO and glass/ITO substrates at temperatures of 125, 150, 200 and 250 °C.

Inverted OSCs with the structure PET/ITO/ZnO/poly(3-hexylthiophene):[6, 6]-phenyl C<sub>61</sub>-butyric acid methyl ester (P3HT:PCBM)/MoO<sub>x</sub>/Ag were fabricated on 50 nm ZnO

coated PET/ITO. For the active layer, a blend of P3HT and PCBM film in a 1:1 weight ratio up to about 280 nm was spray coated on the ZnO film with a **supersonic nozzle (Z95S, Siansonic)**. MoO<sub>x</sub> films (8 nm) and Ag films (80 nm) were then successively thermally evaporated on to the P3HT:PCBM blend below 10<sup>−4</sup> Pa. Current density–voltage (J–V) characteristics were measured using a Keithley 2400 source measure unit. The OSC performance was measured with an Air Mass 1.5 Global (AM 1.5 G) solar simulator and an irradiation intensity of 100 mW cm<sup>−2</sup>.

A precursor for ZnO growth was vacuum-dried at room temperature and then tested using a simultaneous thermal analyzer (STA 449 F3, NETZSCH). The composition and crystal structure were characterized by X-ray diffraction (XRD, PANalytical X'Pert PRO) in grazing incidence mode. The surface morphology of the films was characterized using a scanning electron microscope (SEM, Hitachi S4800). The optical transmittance spectra in the wavelength range of 250–850 nm were recorded using a UV–Vis spectrophotometer (Hitachi U-3900).

## 3 Results and discussion

We conducted a systematic experimental study of the crystal structure, morphology and photovoltaic performance of MICVD derived ZnO buffer layers. The inverted OSCs are shown in Fig. 1a, b. The energy level diagram of the inverted cell is depicted in Fig. 1c [3, 9]. Each group of samples has 24 cells assembled and is tested under the same conditions. The J–V characteristics of the devices with 6 mm<sup>2</sup> active area on Glass/ITO and PET/ITO substrates are shown in Fig. 2a, b. The performance of the OSCs is summarized in Table 1.

For the OSCs based on Glass/ITO substrates, the device with a ZnO CBL deposited at 125 °C shows an open circuit

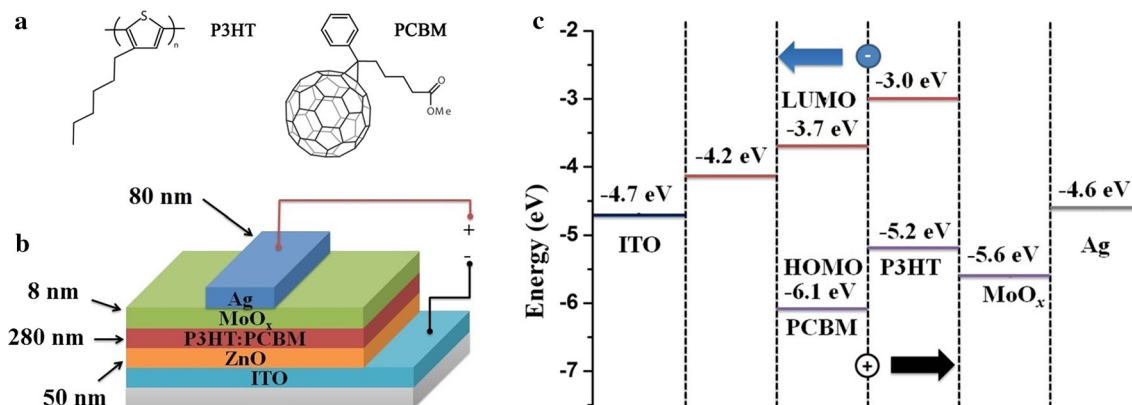


**Fig. 1** a The molecular structures of P3HT and PCBM. b The device structure of the OSC. c Energy level diagram of the component materials used in device fabrication

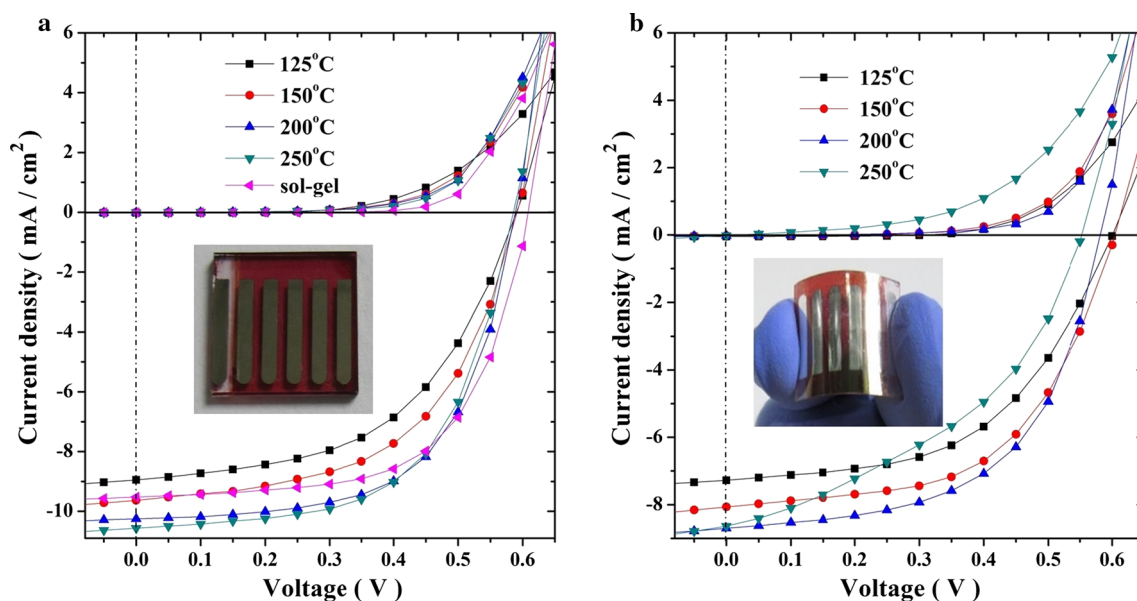


**Fig. 2** J–V characteristics in the dark and under 1.5 M illumination for **a** rigid OSCs and **b** flexible OSCs with ZnO CBLs deposited at different conditions

**Table 1** Important parameters of rigid and flexible OSCs with ZnO CBLs deposited at different conditions

Substrate	ZnO	$V_{OC}$ (V)	$J_{SC}$ (mA/cm <sup>2</sup> )	FF (%)	PCE (%)	$R_S$ ( $\Omega$ cm <sup>2</sup> )	$R_{SH}$ ( $\Omega$ cm <sup>2</sup> )
Glass/ITO	125 °C	0.59	8.95	52	2.7	12	640
	150 °C	0.58	9.63	54	3.1	8	580
	200 °C	0.59	10.25	61	3.7	6	1172
	250 °C	0.59	10.51	59	3.6	7	710
	Sol–gel	0.61	9.52	62	3.6	5	1252
PET/ITO	125 °C	0.60	7.28	52	2.3	19	867
	150 °C	0.60	8.07	55	2.6	11	573
	200 °C	0.58	8.70	56	2.8	8	675
	250 °C	0.55	8.63	42	1.8	10	343

voltage ( $V_{OC}$ ) of 0.59 V, a short circuit current density ( $J_{SC}$ ) of 8.95 mA/cm<sup>2</sup>, a fill factor (FF) of 52 %, and a PCE of 2.7 %. The devices show an increase in  $J_{SC}$  and PCE when the substrate temperature increases to 150 °C. Devices with ZnO CBLs deposited at 200 and 250 °C have very similar performance in PCE. The best device performance was obtained when the substrate temperature was 200 °C, where the PCE was 3.7 % with  $V_{OC}$  of 0.59 V,  $J_{SC}$  of 10.25 mA/cm<sup>2</sup>, and a FF of 61 %. The good performance of rigid OSCs indicates the MICVD deposited ZnO compares favorably with sol–gel derived ZnO as a CBL in small-scale OSCs.

Flexible devices based on PET/ITO substrates exhibit a lower performance with a relatively low  $J_{SC}$  as shown in Fig. 2b and Table 1. We attribute this to the higher square resistance of PET/ITO substrates. The best device performance was also obtained when the substrate temperature was 200 °C. The PCE was 2.8 % with  $V_{OC}$  of 0.58 V,  $J_{SC}$

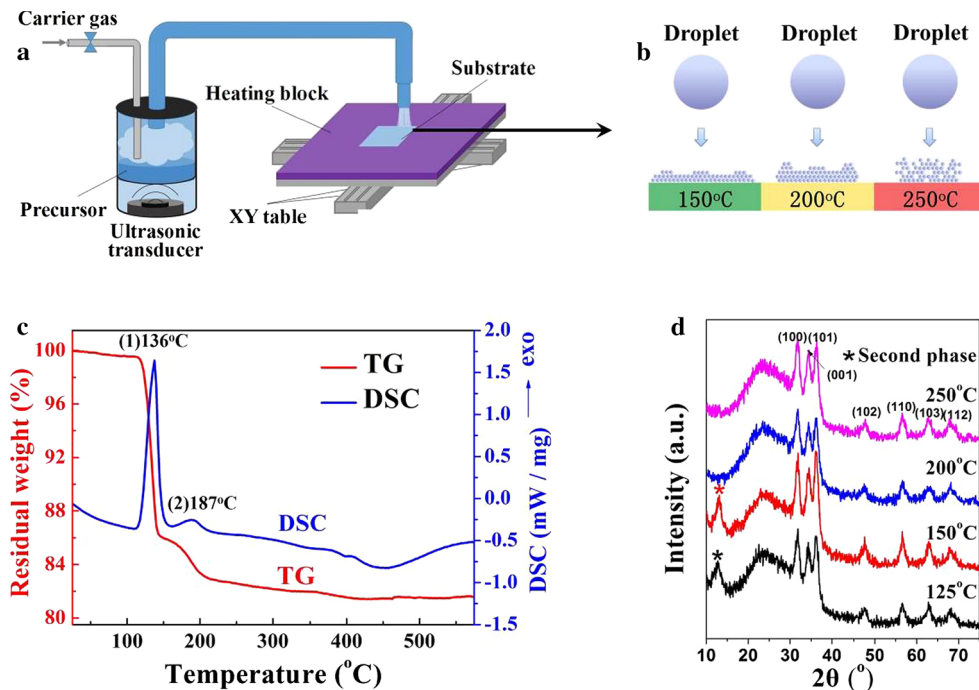
of 8.70 mA/cm<sup>2</sup>, and FF of 56 %. Notice that there is no expected improvement in device performance when substrate temperature increases from 150 to 200 °C. When the substrate temperature increased up to 250 °C, the PCE was only 1.8 %. The gradual degradation in FF and PCE in flexible devices is mainly due to microscopic deformation and crease of PET at the high temperature (~200 °C).

In bulk heterojunctions OSCs, the CBL usually acts as a hole-blocker by collecting negative carriers and thus increasing the shunt resistance of the devices [5, 16]. As shown in Fig. 1c, because the conduction band minimum (CBM) of ZnO is close to the energy of the lowest unoccupied molecular orbital (LUMO) of PCBM, electrons can be efficiently transported to the ITO cathode without significant loss. Generally, well-matched energy levels and a favorable contact interface contribute to excellent charge transport properties and overall performance of OSCs [17, 18]. In fact, the energy levels and interface between the

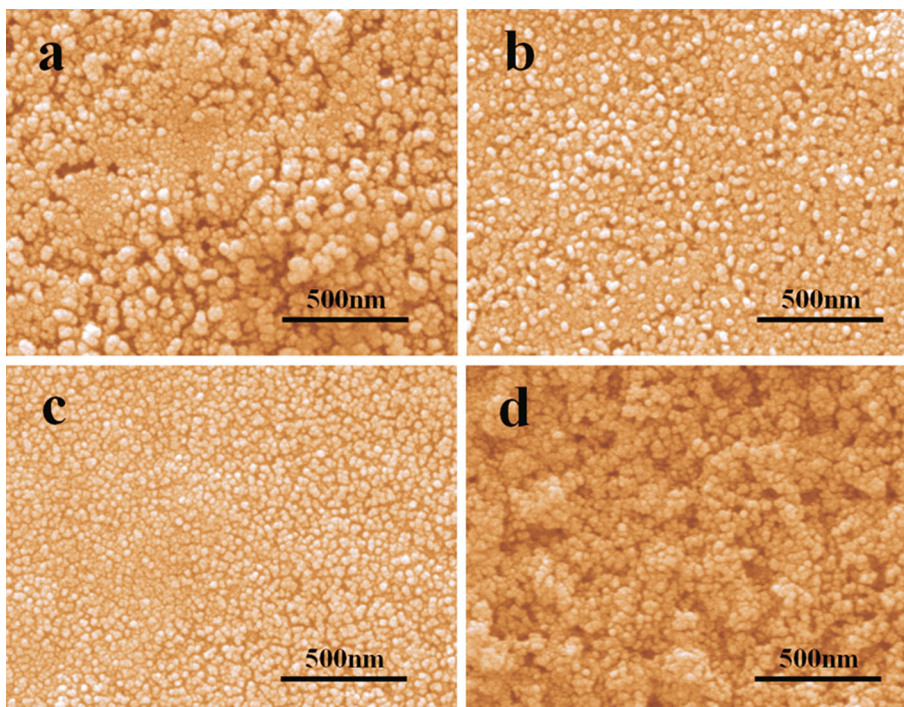
CBL and the active layer depend on the crystal structure and morphology, respectively. For these reasons, the substrate-temperature induced crystal-structure and surface morphology of the MICVD-deposited ZnO film was studied using XRD and SEM to examine their effect on device performance.

The structural properties were observed through XRD patterns of the deposited ZnO at 125, 150, 200 and 250 °C—see Fig. 3d. All of the films have the wurtzite ZnO structure, well-matched with the standard PDF card (No. 36-1451). The three typical crystalline ZnO peaks at 31.8, 34.4, and 36.3 correspond to (100), (002), and (101),

**Fig. 3** **a** Schematic of the MICVD setup. **b** Diagram showing the nano particle growth from droplets at different substrate temperatures. **c** TG and DSC profiles of the ZnO precursor. **d** XRD pattern of ZnO thin films at different substrate temperatures



**Fig. 4** SEM images of ZnO thin films grown at **a** 125 °C, **b** 150 °C, **c** 200 °C and **d** 250 °C



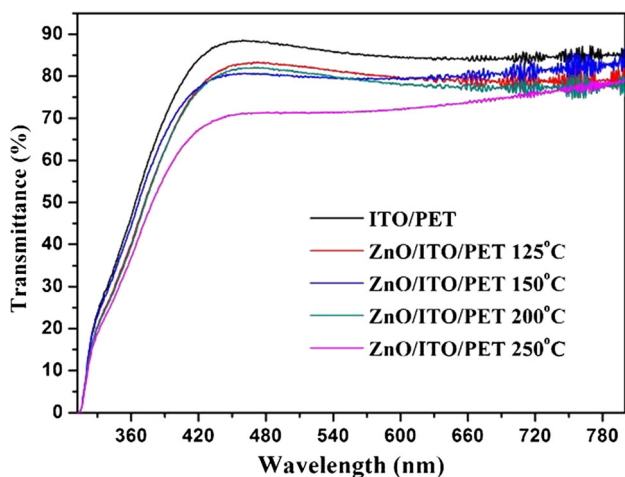


**Fig. 5** Transmittance spectra of ZnO films grown on PET/ITO at different substrate temperatures

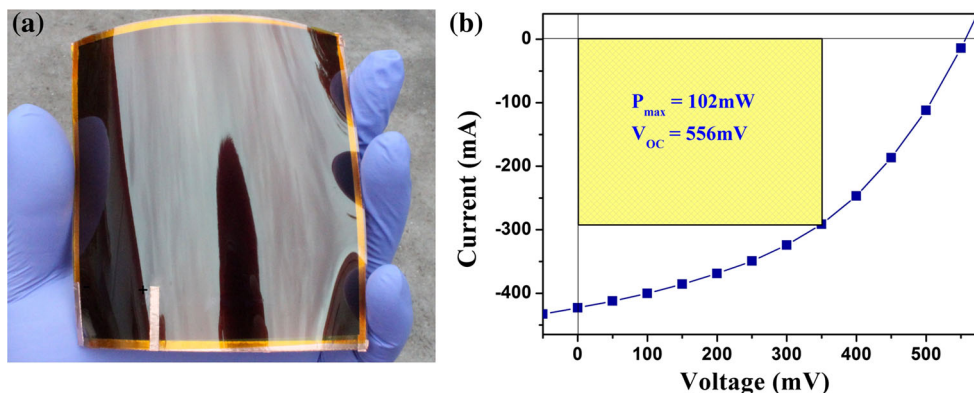
respectively. This indicates superior crystal-quality compared to other low temperature preparation methods [19]. As we can see, there is an amorphous peak at  $12.8^\circ$  in the XRD spectrums of the ZnO film deposited at 125 and 150 °C. This impurity peak disappeared during the increase of the substrate temperature to 200 °C. This peak is very close to the (200) of the zinc acetate standard PDF card (No. 33-1464). We presume that the appearance of this mixed phase is related to a small amount of residual  $\text{CH}_3\text{COO}^-$ . The TG and DSC data indicate similar results. For the dried precursor shown in Fig. 3c, two exothermic reaction peaks at 136 and 187 °C were observed, which indicate that the dried precursor was not pure  $\text{Zn}(\text{OH})_2$ . The weight losses of the two steps were approximately 14 and 3.5 %, respectively, and the total weight loss was about 17 %. The impurity phase produces some negative effects with regard to the electron transport property of ZnO CBL and device performance. It is possible that the charge transport channel between the active layer and the ZnO CBL becomes narrower when redundant acetate mixes with ZnO particles. Thus OSCs with lower temperature

deposited ZnO CBLs had a low current density value—see Table 1.

Different morphologies of ZnO film deposited on PET/ITO substrate at different temperatures were investigated using the SEM surface images shown in Fig. 4. It can be seen that the grain size of the particles decreases with increasing substrate temperature. In particular, the size of particles in ZnO thin films grown at 125 °C is much larger than in other samples, and a porous surface in ZnO films grown at 250 °C can also be observed. A similar phenomenon was found in ZnO films deposited on the PET/ITO substrates. Generally, for spin-coated OSCs, smoother and denser completely covered ZnO layers result in higher performance. This is reflected by the values of FF,  $R_S$  and  $R_{SH}$  [20, 21]. The surface quality of the buffer layer affects directly the morphology of the spin-coated active layer and the contact between them. This affects the photovoltaic performance of the device. Our previous studies have confirmed this [22]. However, as we see in Table 1, the porous morphology has only a small effect on FF and  $R_{SH}$  of for the rigid device. Moreover, the  $J_{SC}$  significantly improved after increasing the roughness. In the same way, devices using ZnO CBL deposited by MICVD show a higher  $J_{SC}$  than that those using the sol-gel method. The reason for the difference is the special active layer deposition process (supersonic spray-coating). The rough ZnO surface has little impact on the deposition of the active layer. The morphology and structure does not depend on the topographic pattern of ZnO. On the other hand, a positive effect is that the rough surface provides a larger contact area between the active layer and the CBL. The charge transport between the active layer and the ZnO CBL improves with reduced energy loss.

This range of morphologies, induced by substrate temperature, can be due to the film growth mechanisms. Before the pyrolysis process, zinc-ammonia solution was atomized into micro-droplets with an average size of approximately 5  $\mu\text{m}$ . When the mist droplets were sprayed onto the hot substrate, the solvent rapidly evaporated and

**Fig. 6 a** Image of a 100  $\text{mm}^2$  flexible OSC device with as-grown ZnO film deposited using MICVD and **b** its current–voltage (I–V) characteristic



the solute crystallized from the solution when it reached the substrate surface—see Fig. 3a, b. Because the low substrate temperature provides only a small driving force for nucleation, the solution had a low nucleation and growth rate. This means the particle can grow much larger. Higher substrate temperatures facilitate a faster nucleation and growth rate. This is also why ZnO thin films grown at high temperature consist of more uniform particles. However, when the temperature is very high (250 °C), the droplet shrinks rapidly and most of the crystal grains grow directly as grown particles. Simultaneously, the solvent evaporates and leaves a shrinkage cavity on the films. The optical performance of ZnO thin films was also affected by the substrate temperature. Figure 5 shows the optical transmittance spectrum of ZnO thin films grown at 125–250 °C. As we can see, the average transmittance of all ZnO thin films grown at 125–200 °C is about 78–80 %, which is a very narrow distribution. When the substrate temperature increases to 250 °C, the optical transmittance suffers from significant degradation. The poor optical performance is due to the large haze that results from the porous morphology.

Based on the above discussion, 200 °C was chosen as the growth substrate temperature to obtain high quality ZnO thin films. Based on the ZnO thin films grown with this technique, a  $100 \times 100 \text{ mm}^2$  flexible OSC with the structure PET/ITO/ZnO/P3HT:PCBM/MoO<sub>x</sub>/Ag was successfully prepared—see Fig. 6a. The I–V characteristics are shown in Fig. 6b. The  $V_{OC}$  and the maximum average power output ( $P_{MAX}$ ) are 556 and 102 mW, which indicates that this low temperature deposition method is suitable for large scale OSCs fabrication. However, the PCE of the flexible solar cells is only about 1 %. The low  $V_{OC}$  and FF are due to the high leakage current caused by the rugged P3HT:PCBM layer rather than the ZnO CBL. In our next work, surface morphology improvement on active layer for flexible OSCs is performed, and the ZnO CBLs deposited by MICVD for efficient larger flexible OSCs will be discussed in detail.

## 4 Conclusions

High density ZnO thin films were successfully grown via MICVD using a zinc–ammonia solution at a very low temperature (125–250 °C). The choice of a suitable substrate temperature is clearly crucial to the composition, morphology, and optical transmittance of ZnO film as well as device performance. 200 °C was the optimal substrate

temperature to achieve high quality ZnO thin film growth. This technique is relative simple, low cost and compatible with large-scale production of flexible organic photoelectric devices.

**Acknowledgments** This work was supported by National Natural Science Foundation of China (Grant No. 61505018), Technology Project from Chongqing Education Committee (Grant No. KJ1401113), Chongqing Science and Technology Commission (Grant No. cstc2013jcyjys50001) and Chongqing University of Science and Arts (Grant Nos. R2012CJ18 and Z2013CJ02).

## References

1. C. Huang, C. Yang, H. Yu, Y. Chen, *J. Appl. Phys.* **115**, 83109 (2014)
2. T. Wu, K. Aw, N.Tjitra Salim, W. Gao, *J. Mater. Sci.: Mater. Electron.* **21**, 125 (2010)
3. Y. Sun, J.H. Seo, C.J. Takacs, J. Seifert, A.J. Heeger, *Adv. Mater.* **23**, 1679 (2011)
4. H.Y. Lee, H.L. Huang, C.T. Lee, *Appl. Phys. Express* **5**, 122302 (2012)
5. R. Po, C. Carbonera, A. Bernardi, N. Camaioni, *Energy Environ. Sci.* **4**, 285 (2011)
6. F. Zhu, X. Chen, L. Zhou, J. Zhou, J. Yang, S. Huang, Z. Sun, *Thin Solid Films* **551**, 131 (2014)
7. C. Periasamy, R. Prakash, P. Chakrabarti, *J. Mater. Sci.: Mater. Electron.* **21**, 309 (2010)
8. H. Cheun, C. Fuentes-Hernandez, Y. Zhou, W.J. Potscavage, S. Kim, J. Shim, A. Dindar, B. Kippelen, *J. Phys. Chem. C* **114**, 20713 (2010)
9. Z. Liang, Q. Zhang, O. Wiranwetchayan, J. Xi, Z. Yang, K. Park, C. Li, G. Cao, *Adv. Funct. Mater.* **22**, 2194 (2012)
10. S.A. Studenikin, N. Golego, M. Cocivera, *J. Appl. Phys.* **83**, 2104 (1998)
11. T.Prasada Rao, M.C.Santhosh Kumar, A. Safarulla, V. Ganesan, S.R. Barman, C. Sanjeeviraja, *Phys. B* **405**, 2226 (2010)
12. J. Xu, H. Wang, L. Yang, M. Jiang, S. Wei, T. Zhang, *Mater. Sci. Eng. B: Adv.* **167**, 182 (2010)
13. S. Seo, S.H. Won, H. Chae, S.M. Cho, *Korean J. Chem. Eng.* **29**, 525 (2012)
14. K. Yoshino, Y. Takemoto, M. Oshima, K. Toyota, K. Inaba, K. Haga, K. Tokudome, *Jpn. J. Appl. Phys.* **50**, 207 (2011)
15. Y. Takemoto, M. Oshima, K. Yoshino, K. Toyota, K. Inaba, K. Haga, K. Tokudome, *Jpn. J. Appl. Phys.* **50**, 8001 (2011)
16. S. Chen, J.R. Manders, S. Tsang, F. So, *J. Mater. Chem.* **22**, 24202 (2012)
17. Y. Jouane, S. Colis, G. Schmerber, A. Dinia, P. Bazylewski, G.S. Chang, Y. Chapuis, *Thin Solid Films* **576**, 23 (2015)
18. P. Morvillo, R. Diana, A. Mucci, E. Bobeico, R. Ricciardi, C. Minarini, *Sol. Energy Mater. Sol. Cells* **141**, 210 (2015)
19. Y.J. Noh, S.I. Na, S.S. Kim, *Sol. Energy Mater. Sol. Cells* **117**, 14 (2013)
20. P.S. Mbule, T.H. Kim, B.S. Kim, H.C. Swart, O.M. Ntwaeaborwa, *Sol. Energy Mater. Sol. Cells* **112**, 6 (2013)
21. S. Shiratori, K. Muraguchi, *Jpn. J. Appl. Phys.* **51**, 95803 (2012)
22. J. Cheng, R. Hu, Q. Wang, C. Zhang, Z. Xie, Z.W. Long, *Int. J. Photoenergy* **2015**, 201472 (2015)